International Journal of Earth, Energy and Environmental Sciences
ISSN: 2517-942X
Vol:12, No:11, 2018

Topping Failure Analysis of Anti-Dip Bedding Rock Slopes Subjected to Crest Loads

Chaoyi Sun, Congxin Chen, Yun Zheng, Kaizong Xia, Wei Zhang

***Abstract*—**Crest loads are often encountered in hydropower, highway, open-pit and other engineering rock slopes. Toppling failure is one of the most common deformation failure types of anti-dip bedding rock slopes. Analysis on such failure of anti-dip bedding rock slopes subjected to crest loads has an important influence on engineering practice. Based on the step-by-step analysis approach proposed by Goodman and Bray, a geo-mechanical model was developed, and the related analysis approach was proposed for the toppling failure of anti-dip bedding rock slopes subjected to crest loads. Using the transfer coefficient method, a formulation was derived for calculating the residual thrust of slope toe and the support force required to meet the requirements of the slope stability under crest loads, which provided a scientific reference to design and support for such slopes. Through slope examples, the influence of crest loads on the residual thrust and sliding ratio coefficient was investigated for cases of different block widths and slope cut angles. The results show that there exists a critical block width for such slope. The influence of crest loads on the residual thrust is non-negligible when the block thickness is smaller than the critical value. Moreover, the influence of crest loads on the slope stability increases with the slope cut angle and the sliding ratio coefficient of anti-dip bedding rock slopes increases with the crest loads. Finally, the theoretical solutions and numerical simulations using Universal Distinct Element Code (UDEC) were compared, in which the consistent results show the applicability of both approaches.

***Keywords*—**Anti-dip slopes, crest loads, stability analysis, toppling failure.

I. Introduction

THE block toppling on rock slopes is often associated with rock masses with transverse fractures which produce blocks of dimension not negligible compared with the slope extension [1]. Toppling failure may occur on various types of rock slopes and even hard soil slopes, as long as the joints in the slope are properly produced. Anti-dip slopes failure is often encountered in hydropower, highway, open-pit and other engineering projects. Such as the excavation slope rock fall in US Brilliant, cut slope toppling failure in San Antolin, Spain [2] and the northern foothills of Vajont, Italy [3].

At present, the theoretical analysis of slope toppling failure mainly includes two different methods: flexural toppling and block toppling. Aydan et al. [4] used the cantilever beam bending model and the limit equilibrium theory to obtain the residual thrust of the anti-dip slope by iterative solution. Based on this force, the stability analysis method was established and validated by indoor model test. Goodman and Bray [5] proposed a step-by-step analysis method for block toppling failure based on the limit equilibrium, which laid the theoretical foundation for block toppling failure. Later, Bobet et al. [6]-[9] developed the block toppling failure analysis methods based on Goodman and Bray [5]. Besides, some scholars [10], [11] used numerical calculation software to analyze the block toppling of the anti-dip slopes and achieved certain results.

Most of the above scholars studied the stability of the slope toppling failure under its own weight. Few scholars have studied the toppling failure mechanism under the crest load. Furthermore, the crest load is a non-negligible factor in the stability analysis of highway, railway and mine slopes. Therefore, the research on the toppling failure mechanism of anti-dip slope subjected to the crest load is of great significance in road and mine slopes engineering.

In many cases, the failure surface of the anti-dip slope is perpendicular to the steeply inclined joint. Many scholars [5], [6], [12], [13] have investigated the slope toppling failure mechanisms and analysis methods under such condition. On this basis, this paper discusses the stability analysis method of the anti-dip slope subjected to the crest load of the slope at the arbitrary angle between the failure surface and the steeply inclined joint. First, the geo-mechanical model of the anti-dip slope subjected to the crest load is established. Then, the formulation for solving the residual thrust of the anti-dip slope by using the transfer coefficient method proposed in [7]. Finally, the influence of the crest load on the stability of the anti-dip slope is analyzed.

II. Toppling Failure Analysis

A. Geological Geometry Model

At present, the geological model of the anti-dip bedding rock slopes is almost always the same. That is, the slopes contain a set of parallel equidistant steeply inclined joints that are consistent with their strikes and are cut by lateral cracks to form discrete rock blocks combinations with a stepped potential failure surface. The stability analysis of such discrete rock blocks combinations is based on a single rock block [14]. In this paper, it is assumed that the crest load is evenly distributed, and the direction is vertically downward, acting on the slope crest,

Chaoyi Sun is with the State Key Laboratory of Geomechanics and Geotechnical Engineering, Institute of Rock and Soil Mechanics, Chinese Academy of Sciences, Wuhan, Hubei CO 430071, China; and University of Chinese Academy of Sciences, Beijing CO 100049, China (e-mail: chaoyisun@126.com).

Congxin Chen, Kaizong Xia, and Wei Zhang are with the State Key Laboratory of Geomechanics and Geotechnical Engineering, Institute of Rock and Soil Mechanics, Chinese Academy of Sciences, Wuhan, Hubei CO 430071, China (e-mail: cxchen@whrsm.ac.cn, kzxia@whrsm.ac.cn, wzhang@whrsm.ac.cn).

Yun Zheng is with the State Key Laboratory of Geomechanics and Geotechnical Engineering, Institute of Rock and Soil Mechanics, Chinese Academy of Sciences, Wuhan, Hubei CO 430071, China (corresponding author, e-mail: yzheng@whrsm.ac.cn).

as shown in Fig. 1.

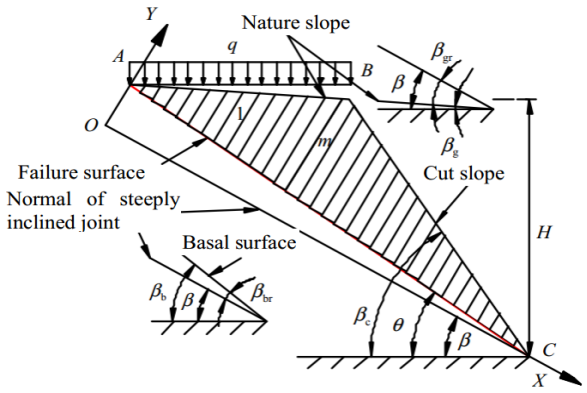

Fig. 1 Geometric geometry model of the toppling failure

For ease of analysis, a coordinate system is established (Fig. 1). The *X*-axis is perpendicular to the steeply inclined joint, that is, the *X*-axis is parallel to the normal direction of the steeply inclined joint. In this figure, the symbol H is used to denote the anti-dip slope height; the symbol θ is used to denote the dip angle of the potential failure surface; the symbols β_g and β_c are used, respectively, to denote the dip angles of the nature slope and the cut slope surfaces; the symbols β and β_b are used, respectively, to denote the dip angles of the normal direction of the steeply inclined joint and the basal surface of the rock block. In addition, the symbols β_{br} β_{gr} β_{cr} and θ_r are some calculating intermediate parameters.

$$\left.\begin{aligned}\beta_{br}&=\beta_b-\beta\\ \beta_{gr}&=\beta-\beta_g\\ \beta_{cr}&=\beta_c-\beta\\ \theta_r&=\theta-\beta\end{aligned}\right\} \tag{1}$$

The premise of the stability analysis on the toppling failure shown in Fig. 1 is that the wedge body *ABC* does not undergo overall sliding failure, that is, the friction angle of the basal surface of the rock block (φ_b) and the dip angle of the basal surface of the rock block (β_b) should satisfy:

$$\varphi_b > \beta_b \tag{2}$$

B. Toppling Failure Criterion for a Single Rock Block

The toppling failure criterion for a single rock block is that the sum of the rotational moments of the crest loads and the weight to the corner point *p* is greater than zero ($M>0$), as shown in Fig. 2.

It can be seen from Fig. 2 that the toppling failure of a single rock block subjected to the crest load must satisfy (3). The rock block is approximately regarded as a parallelogram when calculated.

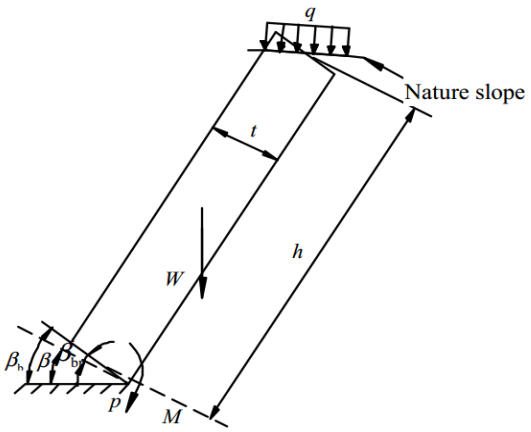

Fig. 2 Stability of a single rock block subjected to crest load

$$\chi \geq \frac{\lambda(1-\tan\beta\tan\beta_{br})+h\cos\beta(1-\tan\beta\tan\beta_{br})}{2\lambda\tan\beta+h\sin\beta} \tag{3}$$

where χ is the height-to-width ratio, namely, $\chi=h/t$, h and t are the height and width of the rock block respectively; λ is the loading ratio, namely, $\lambda=q/\gamma$, q and γ are the loading density and the unit weight of the rock block, respectively.

C. Block Number Determination for the Slope Crest

Starting from the rock block in the first block toppling, the rock block at the crest of the slope is numbered *m*. From the geometric relationship in Fig. 1, the height and height-to-width ratio of the rock block can be determined as:

$$\left.\begin{aligned}h_m&=\frac{H}{\sin\beta_c}\cos\beta_{cr}(\tan\beta_{cr}-\tan\theta_r)\\ \chi_m&=\frac{h_m}{t}\end{aligned}\right\} \tag{4}$$

And then, the height of any blocks is determined as:

$$h_i=\begin{cases}h_m-(m-i)(\tan\beta_{gr}+\tan\theta_r)t & i\leq m\\ h_m+(m-i)(\tan\beta_{cr}-\tan\theta_r)t & i>m\end{cases} \tag{5}$$

Under the crest load, the first toppling block should satisfy (3), namely

$$\chi_1 \geq \frac{\lambda(1-\tan\beta\tan\beta_{br})+h_1\cos\beta(1-\tan\beta\tan\beta_{br})}{2\lambda\tan\beta+h_1\sin\beta} \tag{6}$$

We know that $\chi_1=\frac{h_1}{t}$, so (6) can be rewritten as

$$h_1 \geq \frac{tA_b\cos\beta-2\lambda\tan\beta+K}{2\sin\beta} \tag{7}$$

where, $A_b=1-\tan\beta\tan\beta_{br}$,

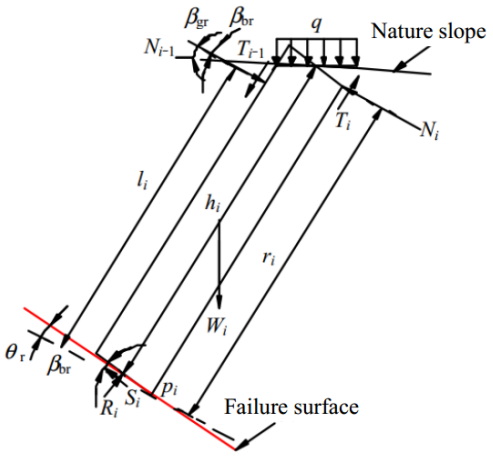

(a) Rock block i located above the slope crest ($i < m$)

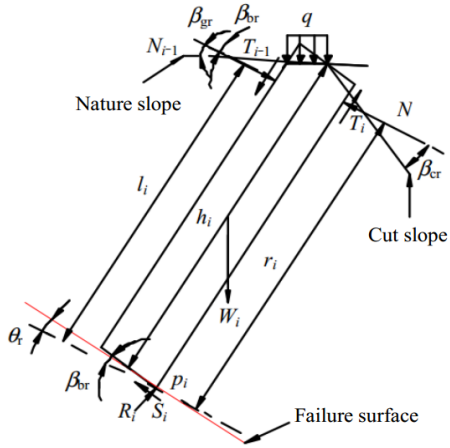

(b) Rock block i located at the slope crest ($i = m$)

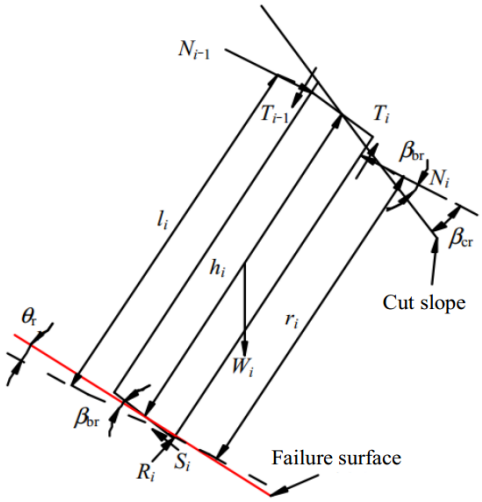

(c) Rock block i located below the slope crest ($i > m$)

Fig. 3 Mechanical model of the slope toppling failure subjected to crest load

$$K = \sqrt{(2\lambda \tan\beta - tA_b \cos\beta)^2 + 4\lambda t A_g \sin\beta}\,.$$

Bring (5) into (7), with the result

$$m \le 1 + \frac{\chi_m}{\tan\beta_{gr} + \tan\theta_r} - \frac{tA_b \cos\beta - 2\lambda \tan\beta + K}{2t(\tan\beta_{gr} + \tan\theta_r)\sin\beta} \tag{8}$$

The m value of the rock block number can be obtained by rounding the right end of (8), and then the number of toppling block above the slope crest can be obtained for given slope subjected crest load. Thus, the effective region for the crest load is determined by combing the position of the first toppling block.

D. Basic Assumptions and Mechanical Models

In the analysis of this paper, the two basic assumptions put forward by Goodman and Bray [5] are still used: (1) frictional limit equilibrium conditions are satisfied at the interfaces of neighboring blocks and (2) the normal forces between blocks are applied at the uppermost point of the intersection of the blocks. Based on these two basic assumptions, the mechanical models of the rock block i subjected to the crest load are divided into three cases, as shown in Fig. 3.

When the rock block i is in the limit rotation equilibrium, the rock block is in contact with the bedrock corner point, and the normal force (R_i) and the shear force (S_i) on the basal surface of the rock block act on the corner point p_i, so no rotational moment is generated for R_i and S_i with respect to the center point p_i. Moreover, the shear force acting on rock block i-1 and i+1 are, respectively, $T_{i-1} = N_{i-1}\tan\varphi_i$ and $T_i = N_i \tan\varphi_i$. Thus, we can give the limit rotation equilibrium equation for rock block i subjected to crest load.

When $i < m$,

$$N_i = \frac{l_i - t\tan\varphi_i}{r_i} N_{i-1} + \frac{1}{r_i}\left(\frac{h_i}{2}\sin\beta - \frac{t}{2}\cos\beta A_b\right)W_i + \frac{1}{r_i}\left(h_i \sin\beta - \frac{t}{2}\cos\beta A_b\right)Q_i \tag{9}$$

When $i = m$,

$$N_m = \frac{l_m - t\tan\varphi_i}{r_m} N_{m-1} + \frac{1}{r_m}\left(\frac{h_m}{2}\sin\beta - \frac{t}{2}\cos\beta A_b\right)W_m + \frac{1}{r_m}\left\{h_m \sin\beta - \frac{t}{4}\cos\beta\left[3 - \tan\beta(2\tan\beta_{br} - \tan\beta)\right]\right\}Q_m \tag{10}$$

When $i > m$,

$$N_i = \frac{l_i - t\tan\varphi_i}{r_i} N_{i-1} + \frac{1}{r_i}\left(\frac{h_i}{2}\sin\beta - \frac{t}{2}\cos\beta A_b\right)W_i \tag{11}$$

where N_{i-1} and N_i are, respectively, the normal force acting

on rock block *i-1* and *i+1*; l_i and r_i are, respectively, the moment arm of the N_{i-1} and N_i. In addition, φ_i is the friction angle of the steeply inclined joint; W_i is the weight of block *i*; Q_i is the crest load acting on rock block *i*, gives

$$Q_i = \begin{cases} \dfrac{qt}{\cos\beta} & i < m \\ \dfrac{qt}{2\cos\beta} & i = m \\ 0 & i > m \end{cases} \tag{12}$$

Equations (9)-(11) can hence be rewritten in the general form

$$N_i = \psi_i N_{i-1} + \xi_i W_i + \zeta_i Q_i \tag{13}$$

where ψ_i, ξ_i and ζ_i are, respectively, the transfer coefficient of the block toppling, weight and crest load, are given as

$$\psi_i = \frac{l_i - t\tan\varphi_i}{r_i} \tag{14}$$

$$\xi_i = \frac{1}{r_i}\left(\frac{h_i}{2}\sin\beta - \frac{t}{2}\cos\beta A_b\right) \tag{15}$$

$$\zeta_i = \begin{cases} \dfrac{1}{r_i}\left(h_i\sin\beta - \dfrac{t}{2}\cos\beta A_b\right) & i \neq m \\ \dfrac{1}{r_i}\left\{h_i\sin\beta - \dfrac{t}{4}\cos\beta\left[3 - \tan\beta(2\tan\beta_{br} - \tan\beta)\right]\right\} & i = m \end{cases} \tag{16}$$

Therefore, the normal force acting on rock block *i+1* are given as

$$N_i = \xi_i W_i + \zeta_i Q_i + \sum_{j=1}^{i-1}\left[\left(\xi_j W_j + \zeta_j Q_j\right)\prod_{k=j+1}^{i}\psi_k\right] \tag{17}$$

Besides, it can be seen from Fig. 3, l_i and r_i are, respectively, given as

$$l_i = \begin{cases} h_i - \tan\beta_{gr} t & i \le m \\ h_i + \tan\beta_{br} t & i > m \end{cases} \tag{18}$$

$$r_i = \begin{cases} h_i & i \le m \\ h_i - \left(\tan\beta_{cr} - \tan\beta_{br}\right) & i > m \end{cases} \tag{19}$$

E. Failure Mode Distinction

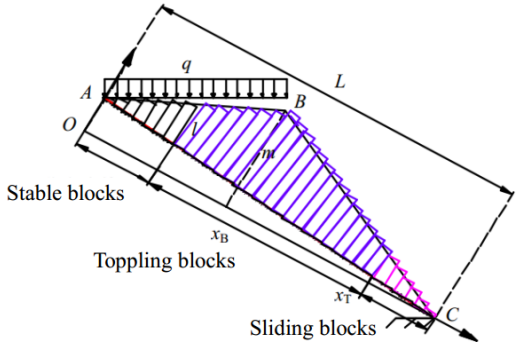

Fig. 4 Schematic of slope failure mode

Due to the small height-to-width ratio of the rock block at the toe of the slope, its anti-toppling stability is strongly good. Thus, sliding failure often occurs instead of toppling failure [5]-[9], as shown in Fig. 4. Liu et al. [7]-[9] pointed out that the position of the slope from the toppling failure to the sliding failure is determined by the force of the basal surface of the rock block. When the sliding force of the rock block is greater than its anti-sliding force (20), the sliding failure will occur. Thus, it should adopt the sliding failure analysis method to analyze the block stability where below this rock block (including this rock block).

$$S_i > R_i\tan\varphi_b \tag{20}$$

Moreover, R_i and S_i can be seen from Fig. 3, given as

$$\left.\begin{aligned} R_i &= \left(W_i + Q_i\right)\cos\beta_b - \left(N_{i-1} - N_i\right)\left(\sin\beta_{br} - \tan\varphi_i\cos\beta_{br}\right) \\ S_i &= \left(W_i + Q_i\right)\sin\beta_b + \left(N_{i-1} - N_i\right)\left(\cos\beta_{br} + \tan\varphi_i\sin\beta_{br}\right) \end{aligned}\right\} \tag{21}$$

Equation (20) can be rewritten as

$$\frac{\left(W_i + Q_i\right)\sin\beta_b + \left(N_{i-1} - N_i\right)\left(\cos\beta_{br} + \tan\varphi_i\sin\beta_{br}\right)}{\left[\left(W_i + Q_i\right)\cos\beta_b - \left(N_{i-1} - N_i\right)\left(\sin\beta_{br} - \tan\varphi_i\cos\beta_{br}\right)\right]\tan\varphi_b} > 1 \tag{22}$$

According to the mechanical analysis of rock block, the normal force between rock blocks can be calculated by (17). At the same time, the normal and shear forces of the block basal surface can be obtained by (21). When the rock block *i* meet the condition shown as (22), the region below this rock block (including this block) should be regarded as the sliding front edge.

To analyze the loading density (q) effect on the failure mode change position, the sliding scale coefficient (κ) is established.

$$\kappa = \frac{n_S}{n_B} \tag{23}$$

where n_S is the number of sliding blocks; n_B is the number of rock blocks located below point *B*, as shown in Fig. 4.

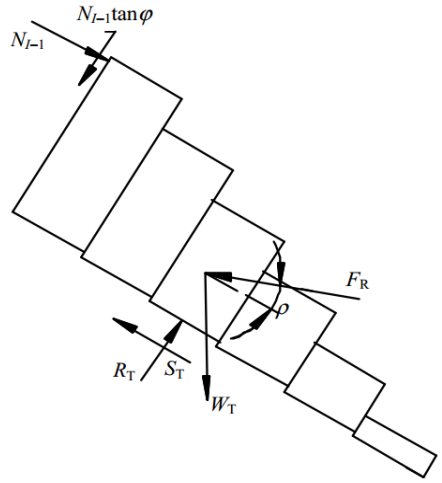

Fig. 5 Mechanical model of sliding front edge

From Fig. 5, the residual thrust of the sliding front edge (P_R) can be written as

$$P_R = \left\{\left[\cos\beta_{br} + \tan\varphi_i \sin\beta_{br} + \left(\sin\beta_{br} - \tan\varphi_i \cos\beta_{br}\right)\tan\varphi_b\right] N_{I-1} + W_T\left(\sin\beta_b - \cos\beta_b \tan\varphi_b\right)\right\} \quad (24)$$

Furthermore, the reinforced force of anti-dip slope can be obtained by the basal surface frictional limit equilibrium of the sliding front edge, gives

$$F_R = \frac{1}{\cos\rho - \tan\varphi_b \sin\rho}\left\{\left[\cos\beta_{br} + \tan\varphi_i \sin\beta_{br} + \left(\sin\beta_{br} - \tan\varphi_i \cos\beta_{br}\right)\tan\varphi_b\right] N_{I-1} + W_T\left(\sin\beta_b - \cos\beta_b \tan\varphi_b\right)\right\} \quad (25)$$

where F_R is the reinforced force; ρ is the angle between the direction of the reinforced force and the basal surface; I is the number of failure mode change position; N_{I-1} is the normal force to keep stable for rock blocks located above the block I ; W_T is the weight of the sliding front edge. What is more, the relationship between the reinforced force and the residual thrust is as

$$F_R = \frac{P_R}{\cos\rho - \tan\varphi_b \sin\rho} \quad (26)$$

F. Summary of the Analysis Process

Based on the limit equilibrium of the block and the transfer coefficient method, the toppling failure analysis process of the anti-dip rock slope subjected the uniform crest load is conducted, as follows:

First, the block will slide if (2) is not satisfied. Instead, the block will topple if (2) is satisfied.

Second, the number of toppling block above the slope crest can be obtained by (8), and then the effective region for the crest load is determined.

Third, the block normal force can be calculated by (17), and the region of the sliding front edge will generate if (22) is satisfied. If so, the basal surface frictional limit equilibrium of the sliding front edge should be conducted. On the contrary, the normal force of the next block will be calculated if (22) is not satisfied.

Finally, the anti-dip slope stability depends on the residual thrust of the sliding front edge (P_R). Slope is stable and does not need reinforce if $P_R \le 0$. However, slope is instable if $P_R > 0$, and the reinforced force can be calculated by (25) or (26).

III. Case Study

The two case examples [2], [13] are used to analyze the effect of different rock block widths and slope cut angles on the slope stability and sliding scale coefficient, which provides the theoretical guidance for the design and support of such slopes. Since the slope geometry parameters and the potential toppling block numbers are adopted to describe the calculating parameters in the slope stability analysis under the crest load, so that the calculating parameters of each toppling block have a unified expression, and the above method is coded into a spreadsheet using Microsoft Excel software to perform toppling analysis efficiently and accurately. The calculation parameters of the two case examples are shown in Table I. Moreover, the basal surface of rock block is perpendicular to the steeply inclined joint ($\beta_{br} = 0$) and the anti-dip slope does not undergo overall sliding failure ($\varphi_b > \beta_b$).

A. Effect of Different Rock Block Widths on the Sliding Scale Coefficient

Figs. 6 (a) and (b) show how the crest load (q) influences the sliding scale coefficient (κ) under the different rock block widths (t).

TABLE I
Calculation Parameters of Case Examples

Cases	H (m)	t (m)	γ (kN/m^3)	β_c (°)	β_g (°)	β (°)	θ (°)	φ_b (°)	φ_i (°)
G-B.1a	92.5	10	25	56.6	4	30	35.8	38.15	38.15
G-B.1b	92.5	10	25	56.6	4	30	35.8	33	33

[a] H = slope height, t = rock block width, γ = rock unit weight, β_c = dip angle of cut slope, β_g = dip angle of nature slope, β = dip angle of the normal of steeply inclined joint, θ = dip angle of potential failure surface, φ_b = friction angle of basal surface, φ_i = friction angle of steeply inclined joint.

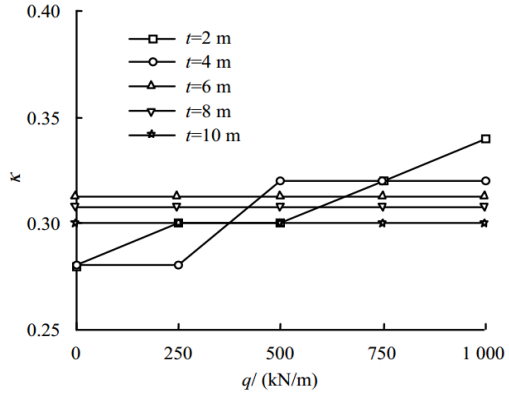

(a) Case G-B.1a

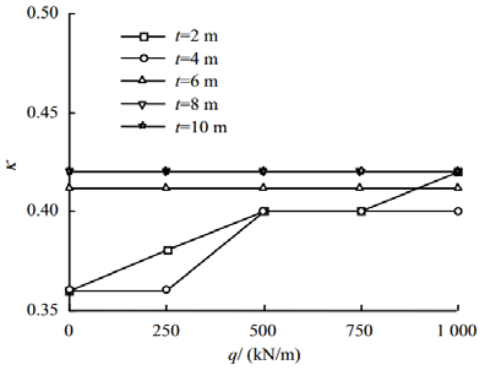

(b) Case G-B.1b

Fig. 6 Curves of crest load vs. sliding scale coefficient

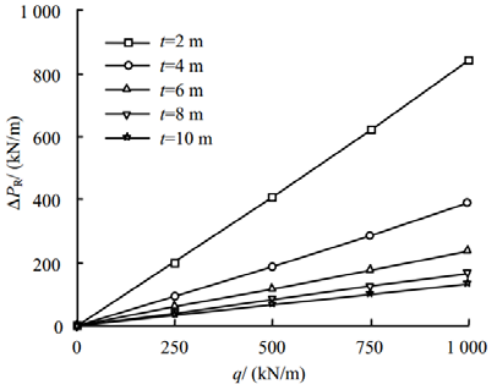

(a) Case G-B.1a

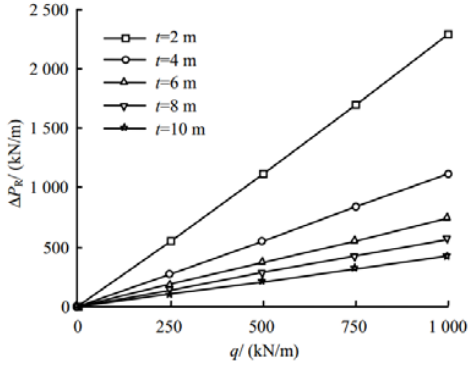

(b) Case G-B.1b

Fig. 7 Curves of crest load vs. residual thrust

It can be seen from Fig. 6, the influence of the crest load (q) on the sliding scale coefficient (κ) is controlled by the rock block width (t). When t is a smaller value, κ nonlinearly increases as q increases. It indicates that the larger crest load, the larger the region of sliding front edge is. However, when t is a larger value, κ almost keeps constant as q increases. Thus, the block width plays a dominant role in the failure mode change position. It implies the greater rock block width, the smaller the effect of the crest load on the failure mode.

B. Effect of Different Rock Block Widths on the Residual Thrust

In the same way, Figs. 7 (a) and (b) show how the crest load (q) influences the residual thrust (P_R) under the different rock block widths (t).

It can be seen from Fig. 7, the residual thrust (P_R) linearly increases as the crest load (q) increases. Furthermore, the smaller rock block width (t), the larger the value of $\mathrm{d}\Delta P_R / \mathrm{d}p$ is. It indicates that the crest load decreases the slope stability. Moreover, the smaller block width, the larger effect of the crest load on the slope stability.

It also can be seen from Fig. 6, a critical rock block width (t_{cr}) or critical average the height-to-width ratio ($\overline{\chi_{cr}}$) does exist. That means that the influence of the crest load on the slope stability in the case of $t \le t_{cr}$ ($\overline{\chi} \ge \overline{\chi_{cr}}$) is more significant than the case of $t > t_{cr}$ ($\overline{\chi} < \overline{\chi_{cr}}$). Besides, the critical rock block width and the critical average the height-to-width ratio are, respectively, 2m and 10 in such both two cases.

C. Effect of Different Slope Cut Angles on the Sliding Scale Coefficient

Keeping the rock block width constant (t = 2m), Figs. 8 (a) and (b) show how the cut angle (β_C) influences the sliding scale coefficient (κ) under the different crest load (q).

As shown in Fig. 8 (a), the sliding scale coefficient (κ) is 0 when the slope cut angle is 45°. Namely, slope (G-B.1a) sliding failure does not occur at that cut angle. Thus, the slope can be self-stabilized by adjusting the cut angle in the excavation design of such slope. In general, it is detected from Figs. 8 (a) and (b) that the larger cut angle, the smaller sliding scale coefficient is. It means the steeper the slope, the smaller the region of the sliding front edge is; instead, the larger region of the block toppling.

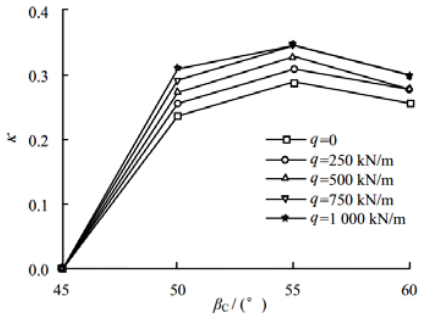

(a) Case G-B.1a

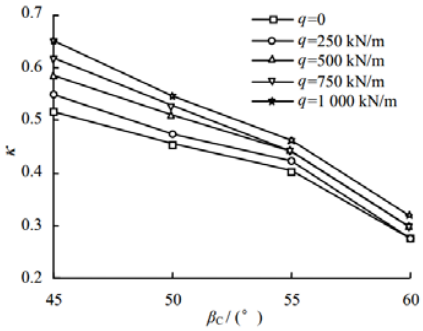

(b) Case G-B.1b

Fig. 8 Curves of cut angle vs. sliding scale coefficient

D.Effect of Different Slope Cut Angles on the Residual Thrust

In the same way, keeping the rock block width constant ($t = 2\text{m}$), Figs. 9 (a) and (b) show how the cut angle (β_C) influence the residual thrust (P_R) under the different crest load (q).

It can be seen from Fig. 9, the increased residual thrust by the crest load (ΔP_R) nonlinearly increases as cut angle (β_C) increases. Slope gradually changes from a stable state to a toppling-sliding failure state with the increase of the cut angle. Namely, cut angle also has significant influence on the slope stability. Therefore, slope can be self-stabilized by adjusting the cut angle in the excavation design of such slope.

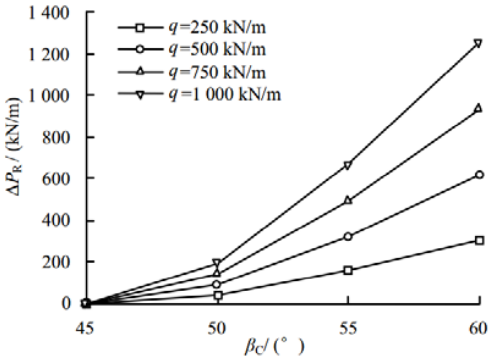

(a) Case G-B.1a

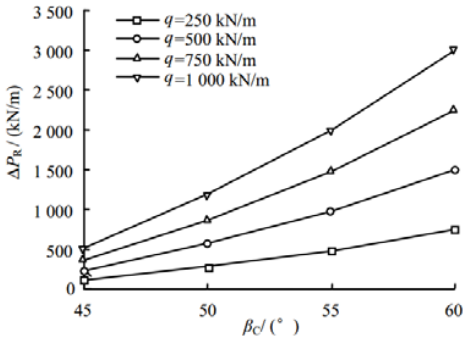

(b) Case G-B.1b

Fig. 9 Curves of cut angle vs. residual thrust

IV. Comparison with Numerical Results

In order to validate the efficacy and accuracy of the new-proposed analysis method, the numerical simulation of the anti-dip slope subjected to crest load is conducted and the theoretical results and the numerical results are compared. Due to space limitations, only one slope (G-B.1a, $t = 2\text{m}$ and $\beta_C = 45°$) is built to conduct comparative analysis. In the numerical simulation, the elastic model is employed for rock blocks and the Coulomb slip model is for joints.

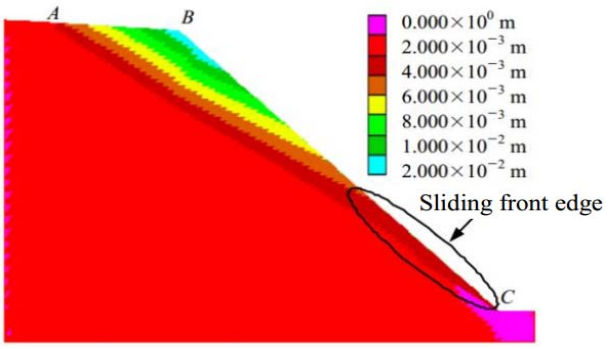

Fig. 10 Horizontal displacement map of slope only subjected weight

From Fig. 10, the horizontal displacement of the bottom and top of the block in the front edge are approximately equal, it indicates that the sliding failure occurs for the block in the front edge. Nevertheless, the horizontal displacement of the top of the block above the front edge is apparently larger than that bottom; it obviously shows the toppling failure characteristics. Thus, adopting the toppling-sliding failure mode to describe such anti-dip slope stability analysis is reasonable.

Fig. 11 shows the distribution of the sliding front edge under crest loads as 0, 500, and 1000 kN/m. It can be detected that the region of the sliding front edge expands from the slope toe to the slope crest as the crest loads increase. It is consistent with the theoretical result.

It can be seen from Fig. 12 that the numerical values of the sliding scale coefficient are a little larger than that theoretical values generally, and the average error for two methods is 11.7%. Furthermore, the smaller value of crest load, the smaller

error is. This is because that the normal forces between blocks are assumed to act on the uppermost point of the intersection of the blocks in the theoretical method, but the acting positions depend on the grids of the interface in the numerical simulation. Anyway, the curve trend of these two methods is the same.

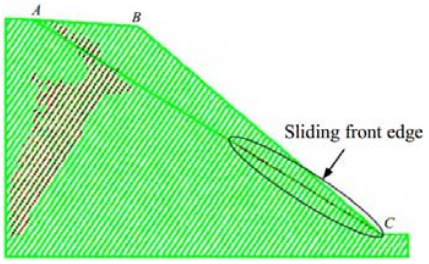

(a) $q = 0$

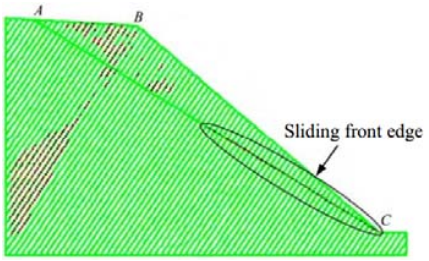

(b) $q = 500$kN/m

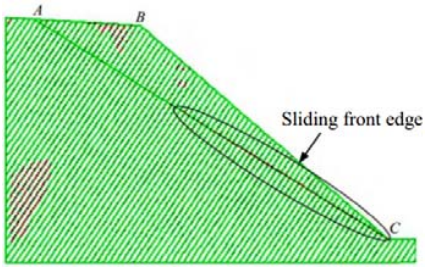

(c) $q = 1000$kN/m

Fig. 11 Distribution of sliding front edge under various crest loads

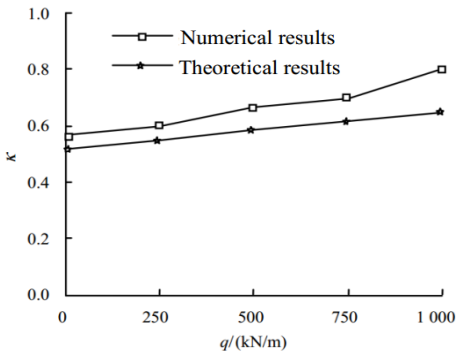

Fig. 12 Comparison of theoretical and numerical results of sliding scale coefficient

In summary, the results of qualitative analysis and quantitative calculation show that the theoretical and numerical results are consistent. On the one hand, the accuracy of the theoretical method for the toppling failure of anti-dip slope subjected crest load is validated. On the other hand, the feasibility of using UDEC to analyze the toppling-sliding failure of the anti-dip slope is also demonstrated.

V. Conclusion

This paper discusses the stability analysis method of the anti-dip slope subjected to the crest load of the slope. Based on the step-by-step analysis approach, a geo-mechanical model was developed, and the related analysis method was proposed for the toppling failure of anti-dip bedding rock slopes subjected to crest loads. Using the transfer coefficient method, a formulation was derived for calculating the residual thrust of slope toe and the support force required to meet the requirements of the slope stability under crest loads. In the end, the theoretical solutions and numerical simulations using UDEC were compared. Our main conclusions can be summarized as follows:

(1) The crest load is a non-negligible factor in the stability analysis. It has significant influence on the slope stability, the position of first block toppling and the region of the sliding front edge.
(2) There exists a critical block width for such slope. The influence of crest loads on slope stability is obvious when the block thickness is smaller than the critical value.
(3) The influence of crest loads on the residual thrust increases with the slope cut angle. Slope can be self-stabilized by adjusting the cut angle in the excavation design of such slope.
(4) The theoretical solutions and numerical simulations using UDEC were compared, in which the consistent results show the applicability of both approaches.

Acknowledgment

We would like to acknowledge the valuable comments and suggestions made by the editor and reviewers. This paper was financially supported by the National Natural Science Foundation of China (grant nos. 11602284, 11472293 and 41807280) and Nature Science Foundation of Hubei Province (grant no. 2018CFB450).

References

[1] F. Lanaro, L. ing, O. Stephansson, G. Barla. “DEM modelling of laboratory tests of block toppling”. *International Journal of Rock Mechanics and Mining Sciences*, 1997, 34, pp. 209-218.
[2] C. Sagaseta, J. M. Sanchez, J. Canizal. “A general analytical solution for the required anchor force in rock slopes with toppling failure”. *International Journal of Rock Mechanics and Mining Sciences*, 2001, 38, pp. 421–435.
[3] L. Muler. “New consideration of the Vajont slide”. *Felsmechnik und Ingenieurgeologie*, 1968, 6, pp. 29－91.
[4] O. Aydan, T. Kawamoto. “The stability of slopes and underground openings against flexural toppling and their stabilization”. *Rock Mechanics and Rock Engineering*, 1992, 25(3), pp. 143－165.
[5] R. E. Goodman, J. W. Bray. “Toppling of rock slopes//Proceedings of ASCE Specialty Conference”, *Rock Engineering for Foundations and Slopes*, Vol.2. Colorado: Boulder, 1976, pp. 201－234.

[6] A. Bobet. “Analytical solutions for toppling failure”. *International Journal of Rock Mechanics and Mining Sciences*, 1999, 36(7), pp. 971–980.
[7] C. H. Liu, M. B. Jaksa, A. G. Meyers. “A transfer coefficient method for rock slope toppling”. *Canadian Geotechnical Journal*, 2009, 46(1), pp. 1–9.
[8] C. H. Liu, M. B. Jaksa, A. G. Meyers. “Toppling mechanisms of rock slopes considering stabilization from the underlying rock mass”. *International Journal of Rock Mechanics and Mining Sciences*, 2008, 45(8), pp. 348-354.
[9] C. H. Liu, M. B. Jaksa, A. G. Meyers. “Improved analytical solution for toppling stability analysis of rock slopes”. *International Journal of Rock Mechanics and Mining Sciences*, 2008, 45(8), pp. 1361-1372.
[10] Y. Zheng, C. X. Chen, X. X. Zhu, Z. Ou, X. M. Xiu, T. T. Liu. “Analysis of toppling failure of rock slopes subjected to seismic loads”. *Rock and Soil Mechanics*, 2014, 35(4), pp. 1025－1032.
[11] D. Y. Sun, Y. J. Peng, X. Z. Wang. “Application of DDA in the analysis of rock slope toppling failure”. *Chinese Journal of Rock Mechanics and Engineering*, 2002, 21(1), pp. 39－42.
[12] M. H. Freitas, R. J. Watters. “Some field examples of toppling failure”. *Geotechnique*, 1973, 23(4), pp. 495－514.
[13] M. Bukovansky, M. A. Rodriguez, G. Cedrun. “Three rock slides in stratified and jointed rocks”. *Advances in rock mechanics*. In: Proceedings of the Third Congress of the ISRM, 1974, pp. 854－862.
[14] C. H. Liu, C. X. Chen. “Analysis of toppling failure of rock slopes due to earthquakes”. *Chinese Journal of Rock Mechanics and Engineering*, 2010, 29(Supp1), pp. 3193－3198.